Durham University

Durham Research Online

Deposited in DRO:

02 December 2015

Version of attached file:

Published Version

Peer-review status of attached file:

Peer-reviewed

Citation for published item:

Sutton, A.D. and Roberts, T.P. and Middleton, M.J. (2015) 'X-ray spectral residuals in NGC 5408 X-1 : diffuse emission from star formation, or the signature of a super-Eddington wind?', Astrophysical journal., 814 (1). p. 73.

Further information on publisher's website:

http://dx.doi.org/10.1088/0004-637X/814/1/73

Publisher's copyright statement:

© 2015. The American Astronomical Society. All rights reserved.

Additional information:

Use policy

The full-text may be used and/or reproduced, and given to third parties in any format or medium, without prior permission or charge, for personal research or study, educational, or not-for-profit purposes provided that:

- a full bibliographic reference is made to the original source
- a link is made to the metadata record in DRO
- the full-text is not changed in any way

The full-text must not be sold in any format or medium without the formal permission of the copyright holders.

Please consult the full DRO policy for further details.

Durham University Library, Stockton Road, Durham DH1 3LY, United Kingdom
Tel : +44 (0)191 334 3042 | Fax : +44 (0)191 334 2971
https://dro.dur.ac.uk

The Astrophysical Journal, 814:73 (9pp), 2015 November 20 doi:10.1088/0004-637X/814/1/73
© 2015. The American Astronomical Society. All rights reserved.

X-RAY SPECTRAL RESIDUALS IN NGC 5408 X-1: DIFFUSE EMISSION FROM STAR FORMATION, OR THE SIGNATURE OF A SUPER-EDDINGTON WIND?

Andrew D Sutton[1,2], Timothy P. Roberts[3], and Matthew J Middleton[4]
[1] Astrophysics Office, NASA Marshall Space Flight Center, ZP12, Huntsville, Al 35812, USA; andrew.d.sutton@nasa.gov
[2] Department of Physics, University of Durham, South Road, Durham, DH1 3LE, UK
[3] Centre for Extragalactic Astronomy, Department of Physics, University of Durham, South Road, Durham, DH1 3LE, UK
[4] Institute of Astronomy, University of Cambridge, Madingley Road, Cambridge, CB3 0HA, UK
Received 2015 June 25; accepted 2015 October 10; published 2015 November 17

ABSTRACT

If ultraluminous X-ray sources (ULXs) are powered by accretion onto stellar remnant black holes, then many must be accreting at super-Eddington rates. It is predicted that such high accretion rates should give rise to massive, radiatively driven winds. However, observational evidence of a wind, in the form of absorption or emission features, has remained elusive. As such, the reported detection of X-ray spectral residuals in *XMM-Newton* spectra of NGC 5408 X-1, which could be related to absorption in a wind is potentially very exciting. However, it has previously been assumed by several authors that these features simply originate from background diffuse plasma emission related to star formation in the ULX's host galaxy. In this work we utilize the spatial resolving power of *Chandra* to test whether we can rule out this latter interpretation. We demonstrate that the majority of the luminosity in these spectral features is emitted from a highly localized region close to the ULX, and appears point-like even with *Chandra*. It is therefore highly likely that the spectral features are associated with the ULX itself, and little of the flux in this spectral component originates from spatially extended emission in the host galaxy. This may be consistent with the suggestion of absorption in an optically thin phase of a super-Eddington wind. Alternatively, we could be seeing emission from collisionally ionized material close to the black hole, but critically this would be difficult to reconcile with models where the source inclination largely determines the observed X-ray spectral and timing properties.

Key words: accretion, accretion disks – black hole physics – X-rays: binaries

1. INTRODUCTION

While it was previously suggested that ultraluminous X-ray sources (ULXs) could contain intermediate mass black holes (Colbert & Mushotzky 1999), several well-developed arguments have been put forward to dispute this (e.g., Grimm et al. 2003; King 2004). Instead, many ULXs may actually be powered by accretion onto stellar-remnant black holes, which has been confirmed in a few cases (e.g., Liu et al. 2013; Middleton et al. 2013; Motch et al. 2014; although at least one ULX contains a neutron star, see Bachetti et al. 2014). Some of these may be more massive than the typical $\sim 10\,M_{\odot}$ stellar-mass black holes that we see throughout our Galaxy, as stellar collapse in regions of low metallicity could leave remnants with masses of up to $\sim 80\,M_{\odot}$ (Zampieri & Roberts 2009; Mapelli et al. 2010). However, the Eddington luminosity of even an $80\,M_{\odot}$ black hole is only $\sim 10^{40}$ erg s^{-1}, and ULXs are observed to exceed this. Hence, if the majority of ULXs do contain stellar-remnant black holes, then many must be accreting matter at close to or in excess of the Eddington limit. It is therefore important to note that high quality ULX X-ray spectra are observed to differ from the standard sub-Eddington states, with many displaying both a soft excess and high energy curvature (e.g., Stobbart et al. 2006; Gladstone et al. 2009; Bachetti et al. 2013).

While the X-ray spectra from ULXs below $\sim 3 \times 10^{39}$ erg s^{-1} are typically broad, disk-like continua, those from more luminous sources have a characteristic two component shape. These peak in either a hard or soft component, in what are termed the hard and soft ultraluminous regimes respectively (Sutton et al. 2013). The hard component may originate in a cool, optically thick corona (Gladstone et al. 2009), or the hot inner disk itself, with a large color correction (Kajava et al. 2012). The soft emission may originate from the base of a radiatively driven wind, which is predicted to arise at super-Eddington accretion rates (Shakura & Sunyaev 1973; Poutanen et al. 2007; Kajava & Poutanen 2009; but see Miller et al. 2013). Although it has previously been mooted that the distinction between these two regimes is largely driven by accretion rate, recent work suggests that the inclination of the ULX is also key (Sutton et al. 2013; Middleton et al. 2015). One potential physical mechanism for introducing the inclination dependence is the super-Eddington outflow, which is expected to be funnel-shaped (Shakura & Sunyaev 1973; Kawashima et al. 2012). While the soft emission is relatively isotropic, the hard emission from the center of the accretion disk can be geometrically beamed by the wind funnel (King 2009). Hence, when viewed close to face-on the hard emission is focussed toward the observer's line of sight and the ULX appears with a hard ultraluminous spectrum. However, at higher inclinations the hard emission is scattered away from the line of sight and the source appears with a soft ultraluminous spectrum. This interpretation is supported by X-ray timing evidence (Sutton et al. 2013), if the edge of the wind is clumpy at its base (Middleton et al. 2011), as is the case in radiation-magnetohydrodynamic simulations (Takeuchi et al. 2013).

One potential test of the funnel-shaped wind model is a search for the signatures of the outflow in ULX X-ray spectra, in the form of absorption and emission lines. In this vein, Walton et al. (2012, 2013) examined the Fe K band in NGC 1313 X-1 and Ho IX X-1, finding that any narrow atomic absorption or emission features must be intrinsically weak or

absent. However, both NGC 1313 X-1 and Ho IX X-1 typically have hard ultraluminous X-ray spectra.[5] In the funnel-shaped wind model the absorbing material would predominantly intercept an observer's line of sight in soft ultraluminous sources, and we would not expect as strong absorption features to be detected in hard ultraluminous sources. Instead, to test the model we ideally want to search for atomic features in soft ultraluminous ULXs, but the requirement for a high count rate makes such an experiment infeasible in the Fe K band in these sources. However, it is potentially very interesting that some soft ultraluminous ULXs do show spectral residuals to their best-fitting continuum models (e.g., Stobbart et al. 2006), including the object that we scrutinize in this paper: NGC 5408 X-1 (2XMM J140319.6−412258; e.g., Strohmayer & Mushotzky 2009; Miller et al. 2013; Middleton et al. 2014).

At a distance of 4.8 Mpc (Karachentsev et al. 2002), NGC 5408 X-1 is one of the best studied ULXs. It has been observed by several of the current generation of X-ray satellites, on a multitude of occasions. Observations include: an *XMM-Newton* large programme (e.g., Pasham & Strohmayer 2012); *Swift* XRT monitoring (Kaaret & Feng 2009; Grisé et al. 2013); and eight *Chandra* exposures, which we re-analyze here. The flux variability of the source rules out an X-ray supernova remnant and confirms that it is powered by accretion onto a compact object (Kaaret et al. 2003; Soria et al. 2004). It persistently displays a distinct soft ultraluminous two component X-ray spectrum in *XMM-Newton* data (Sutton et al. 2013) at an average 0.3–10 keV unabsorbed luminosity of $\sim 1.1 \times 10^{40}$ erg s^{-1} (Strohmayer 2009; although we note that they fit the high energy spectrum with a soft power-law, so may over-estimate the intrinsic luminosity, cf. Middleton et al. 2014). Additional soft residuals have been detected in the *XMM-Newton* spectra which can be well modeled as thermal plasma emission (Strohmayer & Mushotzky 2009; Miller et al. 2013; Middleton et al. 2014). It has previously been assumed that these were the result of diffuse star formation related emission in the host galaxy (Strohmayer et al. 2007; Strohmayer & Mushotzky 2009; Miller et al. 2013). However, we know from observational studies of galaxies that the X-ray luminosity of such emission is correlated with star formation rate ($L_{0.5-2\,\mathrm{keV}}/\mathrm{SFR} \approx 8.3 \times 10^{38}$ erg s^{-1} $(M_\odot\ \mathrm{yr}^{-1})^{-1}$; Mineo et al. 2012), and Middleton et al. (2014) contend that the luminosity of the putative thermal plasma emission ($\sim 2.5 \times 10^{38}$ erg s^{-1}, calculated from Miller et al. 2013) greatly exceeds that inferred from star formation, even over the entirety of NGC 5408 ($\approx 3 \times 10^{37}$ erg s^{-1}, calculated from a 24 μm flux density of 0.42 ± 0.04 Jy, Dale et al. 2005). Instead, Middleton et al. (2014) show that the putative plasma emission features could actually be commensurate with broadened, blueshifted absorption in a partially ionized, optically thin medium. Such a medium would be expected to occur in a super-Eddington wind, as it becomes optically thin at large distances ($>10^3 R_g$) from the central black hole.

[5] One of the *XMM-Newton* observations of NGC 1313 X-1 analyzed by Walton et al. (2013) was classified as soft ultraluminous and a second as ambiguous (either hard of soft ultraluminous) by Sutton et al. (2013). However, out of a total of 164 ks of good time in the EPIC pn detector analyzed by Walton et al. (2013), these observations only contributed 9 and 10 ks respectively. A further observation with 3 ks of good EPIC pn time was not classified by Sutton et al. (2013). As such, the vast majority of the NGC 1313 X-1 data studied by Walton et al. (2013) comes from epochs when the source had a hard ultraluminous spectrum.

In this paper, we utilize *Chandra* archival data to determine the spatial origin of the soft plasma emission-like features in the X-ray spectrum of NGC 5408 X-1. The high angular resolution of *Chandra* is absolutely key to this analysis. Having constrained the spatial origin of these spectral features, we are able to make important inferences as to their nature. In Section 2 we examine the spatial and spectral properties of the ULX and surrounding regions in *Chandra* ACIS data, and interpret these results in Section 3.

2. ANALYSIS AND RESULTS

Before examining the *Chandra* X-ray observations of NGC 5408 X-1, we briefly consider the optical/UV data. NGC 5408 X-1 is located around ∼12 arcsec from the major regions of star formation in NGC 5408 (Figure 1; Kaaret et al. 2003). This would fall well within a typical *XMM-Newton* source extraction region centered on the ULX, thus star formation related emission could feasibly contaminate the X-ray spectrum. However, NGC 5408 X-1 is sufficiently displaced from these star formation regions that *Chandra* ACIS can spatially resolve them from the ULX. There is a much smaller stellar association containing ∼20 OB stars, located around 4 arcsec north east of NGC 5408 X-1 (Grisé et al. 2012), and this may still slightly contaminate the *Chandra* spectrum of the source.

The region around NGC 5408 has been observed with *Chandra* on a total of nine occasions, eight of which are suitable for studying X-1. In this work, we analyze these eight observations, which were taken using the 1/8 sub-array of ACIS-S, with X-1 being positioned close to on-axis. In the case of NGC 5408 X-1, the use of the 1/8 sub-array is critical to mitigate the effects of pileup. We estimate residual pileup fractions of ∼5% based on PIMMS (v4.7b: with ACIS Pile up and Background Count Estimation)[6] simulations of an absorbed power-law with parameters from Gladstone et al. (2009) and an unabsorbed 0.3–10 keV luminosity of 1.1×10^{40} erg s^{-1} (Strohmayer 2009). Details of the observations included in this work are given in Table 1, and a combined exposure map is shown in Figure 2. We downloaded each dataset from the HEASARC archive,[7] and analyzed them using tools in CIAO 4.6,[8] with calibration database 4.6.3. We note that we would not expect the analysis to change significantly if CIAO 4.7 was used instead.

The first stage of the analysis was to confirm that the ULX appeared point-like at the spatial resolution of *Chandra*. To do this, the individual observations were reprocessed using the CHANDRA_REPRO script, before being stacked using MERGE_OBS. The stacked image is shown in Figure 3, where it has been divided by the total exposure map of the *Chandra* observations (with 8 × 8 pixel binning). A number of faint point sources are evident, which would be confused with the ULX in typical 30 arcsec *XMM-Newton* source extraction regions.

We applied the SRC_EXTENT script to the individual observations to determine whether NGC 5408 X-1 is extended. In preparation for this, we simulated the *Chandra* ACIS-S point-spread function (PSF) for each observation using CHART (*Chandra* ray tracer)[9] and the MARX (model of *AXAF* response to X-rays version 5.0.0; Davis et al. 2012) software suite. As

[6] http://cxc.harvard.edu/toolkit/pimms.jsp
[7] http://heasarc.gsfc.nasa.gov
[8] http://cxc.harvard.edu/ciao/
[9] http://cxc.harvard.edu/chart/

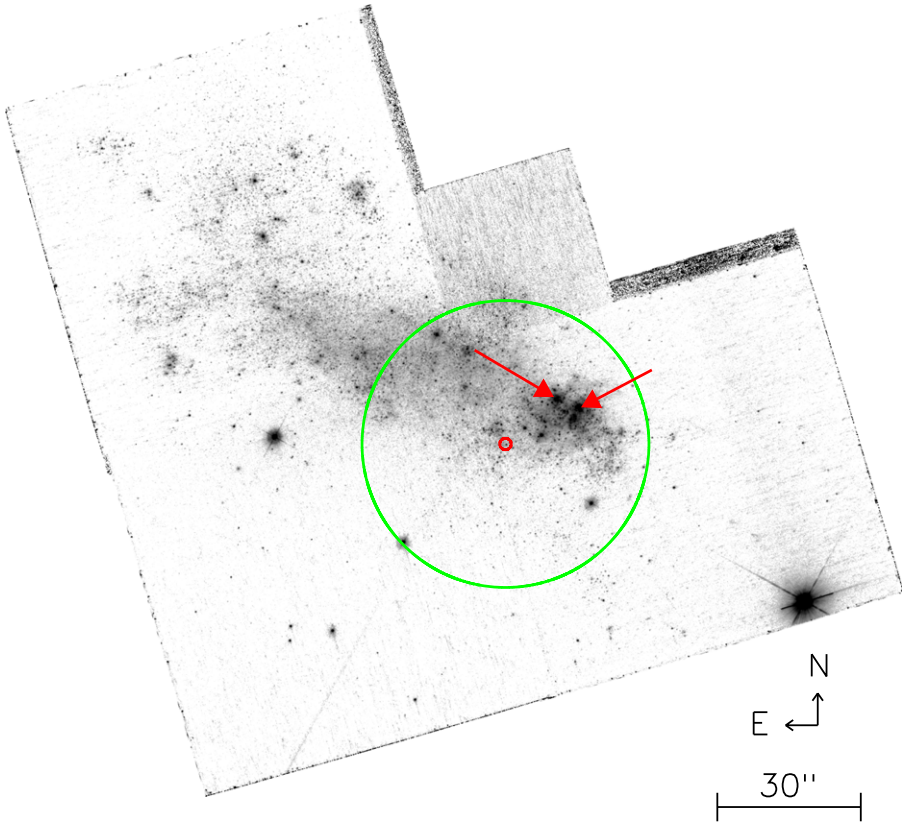

Figure 1. *HST* WFPC2 image in the F336W near-UV filter of NGC 5408, downloaded from the Hubble Legacy Archive. The position of NGC 5408 X-1, taken from the *Chandra* Source Catalog (Evans et al. 2010), is indicated by the arbitrarily sized red circle, while the larger green circle corresponds to a nominal 30 arcsec *XMM-Newton* source extraction region centered on the ULX. Clearly the ULX is not embedded in a young stellar association, where star formation related diffuse emission would be expected. Instead, it is located about ∼12 arcsec from the major regions of star formation in the galaxy (Kaaret et al. 2003; red arrows). Diffuse emission from these regions may contaminate the *XMM-Newton* spectrum of NGC 5408 X-1, but can trivially be spatially resolved from the ULX by *Chandra* ACIS.

Table 1
Chandra ACIS-S Observations of NGC 5408 X-1

Obs ID	Date (yyyy-mm-dd)	Exposure Time (ks)
4555	2003 Dec 20	5.2
4556	2004 Feb 09	4.9
4557	2004 Dec 20	5.1
4558	2005 Jan 29	5.2
11032	2010 May 02	12.2
11033	2010 May 15	12.2
11034	2010 May 28	12.0
13018	2010 Sep 12	12.0

Note. Details of the *Chandra* ACIS-S observations of NGC 5408 X-1 taken with the 1/8 sub-array.

inputs to CHART, we used the off-axis angles, azimuthal angles and exposure times from each observation, along with absorbed power-law model spectra. These model spectra were fitted to the point source spectra (see below for details of the spectral extraction) in the 0.3–10 keV energy range using SHERPA, and extracted in an appropriate format using the SAVE_CHART_SPECTRUM tool from the CHART_SPECTRUM contributed SHERPA package. The simulated PSFs and the reprocessed event files from each observation were used as inputs to SRC_EXTENT. This script estimates the size of a source using the Mexican Hat Optimization algorithm, and compares this with a PSF. In all but one case, this analysis indicated that the source was

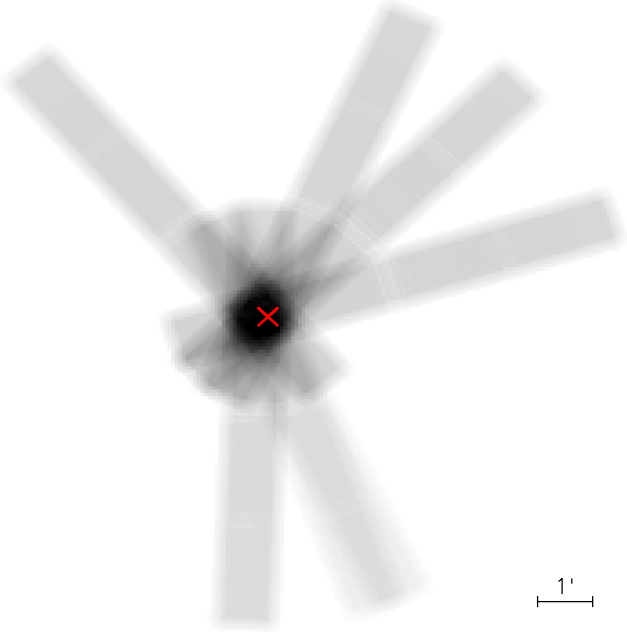

Figure 2. Exposure map of the merged *Chandra* observations. The approximate location of NGC 5408 X-1 is indicated by the red cross. As the ULX is close to the nominal ACIS-S aim-point in all of the observations, their individual footprints all overlap at the position of the target.

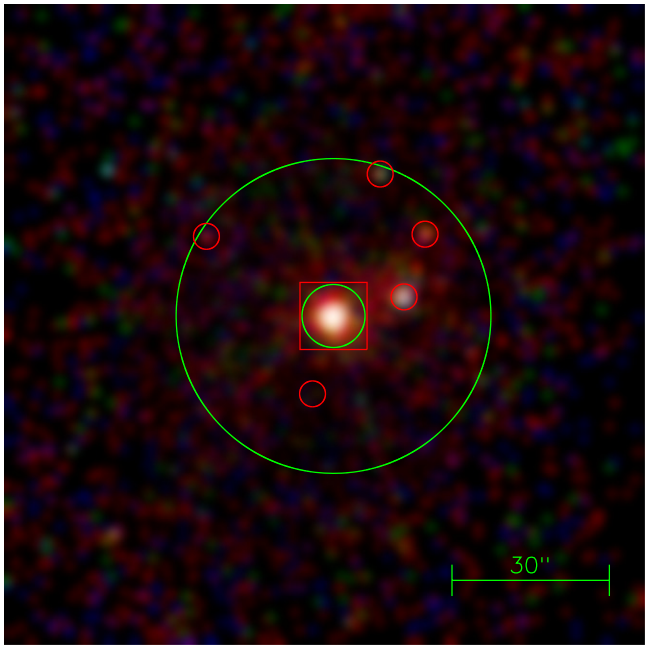

Figure 3. Three-color *Chandra* ACIS-S image of NGC 5408 X-1 and the surrounding regions, centered on the ULX. The RGB colors correspond to 0.2–1.5 keV, 1.5–2.5 keV and 2.5–8.0 keV respectively. To create the image, all eight observations reported in Table 1 were stacked, and the resulting image was divided by the total exposure map (with 8 × 8 pixel binning), before being convolved with a 2.4 arcsec FWHM Gaussian to smooth the final image. The green annulus shows the 6–30 arcsec region in which we estimated the extended emission, and the red box corresponds to the footprint of Figure 4. The smaller, arbitrarily sized red circles show the location of other sources detected by WAVDETECT within 30 arcsec of X-1.

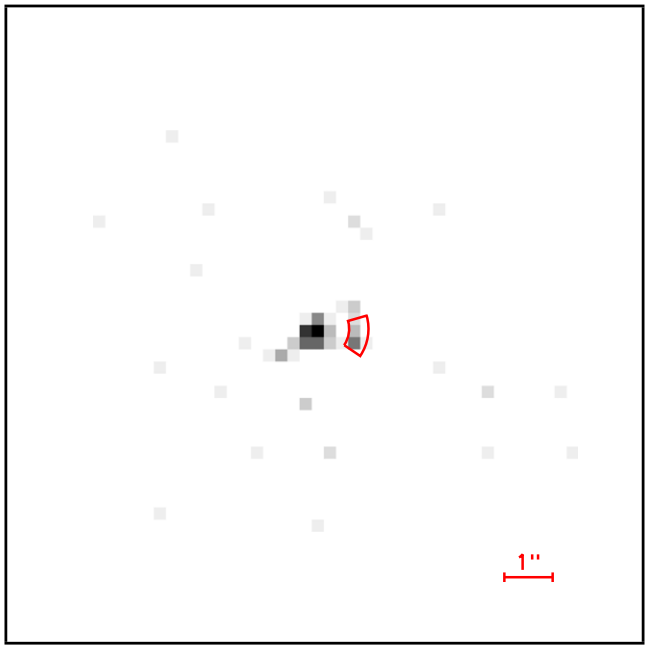

Figure 4. *Chandra* ACIS-S 0.5–8 keV image centered on NGC 5408 X-1 from observation 11034. The displayed image is 26 × 26 native *Chandra* ACIS pixels in size, and has been rebinned to 0.5 pixels. It has been restored using the ARESTORE tool in CIAO with a simulated PSF and 100 iterations of the Lucy–Richardson deconvolution algorithm. The region highlighted in red corresponds to a known asymmetry in the *Chandra* PSF, so the excess of counts here is unlikely to be a real source. Apart from the ULX itself and this PSF asymmetry, no sources were detected by WAVDETECT with greater than 10 counts.

consistent with having zero intrinsic size. The sole exception to this was observation 11034, which had an estimated intrinsic size of $0.14^{+0.05}_{-0.04}$ arcsec (which is not flagged as extended by SRCEXTENT at the default threshold criteria, and we note that the PSF and observed source sizes are consistent at the 90% significance level).

In order to further examine the potential extended emission in observation 11034 on finer scales, we used ARESTORE in CIAO to deconvolve the observed data with a simulated PSF. For this purpose, we created a PSF using CHART and MARX with 10 times the exposure time of the real observation. The CHART raytraces are deterministic rather than statistical, so increasing the number of photons improves our sampling of the PSF. Images of both the observed data and the simulated PSF were created with 0.5 pixel binning. These were used as inputs to ARESTORE, which restores images which have been degraded by a blurring function using the Lucy–Richardson deconvolution algorithm (Richardson 1972; Lucy 1974). We ran the deconvolution algorithm for 100 iterations, after which some additional structure was evident around ∼0.7 arcsec to the west of the ULX (Figure 4). However, this region corresponds to a known asymmetry fixed in spacecraft coordinates,[10] and the excess of counts is highly likely to be this artefact. To test for any other significant resolved sources we ran WAVDETECT on the restored image, with wavelet radii of 1, 2 and 4 image pixels. Apart from the ULX itself and the known artefact, no other sources with greater than 10 counts were detected in the region shown in Figure 4. As such, we find no convincing evidence that the ULX can be further spatially resolved by *Chandra* ACIS.

In addition to the spatial analysis, we also looked for an excess of spectral counts in the regions surrounding the *Chandra* point source, to further test whether the putative plasma emission component could originate there. We fit this emission with a variety of models, a summary of which is given in Table 2. We note that the nature of the features in the *XMM-Newton* spectrum is not clear, and they may originate from either emission or absorption. Throughout the rest of this work we model them as plasma emission, but do not intend to imply that this is the correct physical interpretation. Since the response of *Chandra* ACIS changed significantly during the 7 year time span over which the observations were taken, especially at low energies, it is not acceptable to simply extract a merged spectrum. As such, we used SPECEXTRACT in CIAO to extract energy spectra from each observation in a 6–30 arcsec annular region centered on NGC 5408 X-1 (Figure 3), with appropriate parameters for an extended source (CORRECTPSF = no and WEIGHT = yes). It is clear from Figure 3 that several point sources were resolved by *Chandra* within ∼30 arcsec of NGC 5408 X-1. As such, we used WAVDETECT with SCALES = "1, 2, 4, 8, 16" and SIGTHRESH = 1×10^{-5} (i.e., ∼1 false detection over the number of pixels in the image) to identify sources near to X-1. Sources within 30 arcsec of the ULX are highlighted in Figure 3, and were masked out when defining the extended source region. The SPECEXTRACT script also produces appropriate response matrix files (RMFs), ancillary response files (ARFs) and background spectra, which were estimated from a large circular region, far from the ULX.

[10] http://cxc.harvard.edu/ciao/caveats/psf_artifact.html

Table 2
Spectral Models Used to Fit the Extended Emission

Model[a]	E Range[b]	Mask[c]	Goodness-of-fit[d]
TBABS × MEKAL	0.3–2 keV	y	94%
TBABS × MEKAL[e]	0.3–2 keV	y	76%
TBABS × MEKAL	0.3–2 keV	n	99%
TBABS × (MEKAL + TBABS × POWERLAW)	0.3–10 keV	n	97%

Notes. Summary of the goodness-of-fit statistics for spectral models simultaneously fitted to the extended emission from all of the *Chandra* observations. All model parameters were assumed to be invariable between observations. We note that from a comparison of the first and second models it seems that fixing a parameter of the model to a non-optimal value actually improves the goodness of fit. This is because different fit and test statistics were used.
[a] XSPEC model fitted to the extended spectrum.
[b] Energy range in which the model was fitted.
[c] Flag for whether a point source mask was applied when extracting the extended spectrum, to remove contaminating emission from resolved point sources.
[d] Goodness of fit of the model in terms of the percentage of 10,000 simulated realizations based on the model which had improved Anderson–Darling statistics compared to the real data.
[e] Unlike the other models, here the MEKAL temperature is fixed to the value given in Miller et al. (2013).

The unbinned extended source spectra, RMFs, ARFs and background spectra were read in to XSPEC (version 12.8.1), and simultaneously fitted with a plasma emission model in the 0.3–2 keV energy range. When fitting the model there were insufficient data in each observation to allow us to use binning and the χ^2 statistic, so we used the modified Cash statistic in XSPEC, which allows for a background spectrum to be subtracted.[11] Specifically, the spectral model that we used was TBABS × MEKAL. The absorption component was fixed to the Galactic value (5.93×10^{20} cm^{-2}; Dickey & Lockman 1990) and we used the solar abundance table of Wilms et al. (2000). As any extended emission would not be expected to vary significantly between observations, the MEKAL temperature and normalization were fixed between the spectra. To assess the goodness-of-fit, we used the GOODNESS command in XSPEC to simulate 10,000 realizations from the best fitting model, and calculated the Anderson–Darling statistic to compare these with the real data. Of the 10,000 realizations, 94% had an improved fit-statistic compared to the real data, indicating that the model cannot be rejected at 95% significance (equivalent to 2σ for Gaussian distributed data). This model had a plasma temperature of 0.64 ± 0.03 keV, which is in disagreement with the value of 0.87 ± 0.02 keV reported by Miller et al. (2013) for a plasma emission spectrum fitted to the residual features in *XMM-Newton* EPIC data. However, when we repeated the above goodness-of-fit test with the MEKAL temperature fixed at 0.87 keV, we found that this variant of the model cannot be rejected at high significance either (76% of 10,000 simulated data sets had a lower Anderson–Darling test statistic; note that the test statistic differs from the fit statistic). We used the CFLUX convolution model in XSPEC to estimate the observed 0.3–2 keV flux of the extended emission, integrated over the annular region as $(2.5 \pm 0.2) \times 10^{-14}$ erg cm^{-2} s^{-1}. At the distance of NGC 5408, this is equivalent to a 0.3–2 keV luminosity of $(7.0 \pm 0.5) \times 10^{37}$ erg s^{-1}. If we renormalize this to account for the difference in region size between our annular region with point source masks and a 30 arcsec circle, then this is increased by ∼6% to $(7.4 \pm 0.5) \times 10^{37}$ erg s^{-1}. This is ∼1/3 of the MEKAL flux seen in the *XMM-Newton* data.

The *XMM-Newton* source extraction region does not exclude the faint point sources resolved by *Chandra*, so we test whether these could be contributing any of the missing MEKAL flux. To do this, we repeated the above analysis in the same annular region without masking out the point sources. An absorbed MEKAL model could not be rejected at the equivalent of 3σ significance in the 0.3–2 keV range (99% of 10,000 simulated spectra had an improved fit statistic). We estimated the observed 0.3–2 keV flux using the CFLUX model in XSPEC to be $(3.2 \pm 0.2) \times 10^{-14}$ erg cm^{-2} s^{-1} integrated over the annulus. After correcting for the difference in region size, this is around 20% higher than the previous estimate with point sources excluded, but it still can only account for ∼37% of the *XMM-Newton* MEKAL luminosity. However, when we tried adding a power-law to the spectral model (TBABS × (MEKAL + TBABS × POWERLAW) in XSPEC, with the model fitted in the 0.3–10 keV range, and having a rejection probability of 97%) this resulted in a larger increase in the estimated 0.3–2 keV observed flux. Most of the difference in observed flux between the two models is in the 1–2 keV energy band, and it is likely due to fitting the models over different energy ranges. For the latter model the total observed flux was $(4.7 \pm 0.3) \times 10^{-14}$ erg cm^{-2} s^{-1}, but only $(1.1 \pm 0.4) \times 10^{-14}$ erg cm^{-2} s^{-1} originated in the MEKAL component. As such, much of the faint flux would have been confused with the continuum spectrum in *XMM-Newton*, not the putative plasma emission features. Since the MEKAL flux here is lower than our estimate with the point sources excluded, this may suggest that there is still some unresolved faint point source emission. We therefore take $(7.4 \pm 0.5) \times 10^{37}$ erg s^{-1} as a conservative estimate of the extended contribution to the *XMM-Newton* MEKAL component luminosity, but caution that it should be considered as an upper-limit.

We also examined point source spectra from the ULX to test whether there was evidence of MEKAL-like features, which could indicate that the spectral features have a localized origin close to the ULX. A summary of models fitted to the ULX spectra is given in Table 3. Again, we used SPECEXTRACT in CIAO to extract the source and background spectra, RMFs and ARFs from each of the *Chandra* observations. Source spectra were extracted from 5 arcsec circular regions centered on the ULX, and background spectra from large, circular regions located on the same chip, away from the ULX and other point sources. As is appropriate for a point source, we used parameters CORRECTPSF = yes and WEIGHT = no. The spectra and associated files were grouped and binned to a minimum of 20 counts per energy bin by the SPECEXTRACT script, allowing us to use the χ^2 statistic.

[11] http://heasarc.gsfc.nasa.gov/xanadu/xspec/manual/XSappendixStatistics.html

Table 3
Spectral Models Used to Fit the ULX

Model[a]	χ^2. dof
TBABS × TBABS × POWERLAW	716.7/623
TBABS × (TBABS × POWERLAW + MEKAL)	622.4/621
TBABS × TBABS × SIMPL × DISKBB	628.2/607
TBABS × (TBABS × SIMPL × DISKBB + MEKAL)	615.5/605
TBABS × (TBABS × SIMPL × DISKBB + MEKAL)	617.7/606
TBABS × TBABS × (SIMPL × DISKBB + MEKAL)	613.5/612

Notes. Summary of the goodness-of-fit statistics for a variety of spectral models simultaneously fitted to all of the *Chandra* ULX spectra. In all of the models the first absorption component was set equal to the Galactic neutral hydrogen column density in the direction of the source. The second absorption component was left free to model intrinsic absorption in the source/absorption in the host galaxy. This was free to vary between observations, except in the final model where it was assumed to be invariable. Similarly, ULX components in all of the models (POWERLAW, SIMPL and DISKBB) were allowed to vary between observations, while the MEKAL parameters was assumed to be invariable.
[a] XSPEC model fitted to the extended spectrum.

We read all of the grouped *Chandra* point source spectra into XSPEC and simultaneously fitted them with a simple phenomenological model of emission from a ULX, a doubly absorbed power-law (TBABS × TBABS × POWERLAW in XSPEC). The first absorption component was fixed to the Galactic value, and the second was left free to model intrinsic absorption in the host galaxy and/or the ULX itself. The power-law spectral index and normalization were allowed to vary between observations, to model any spectral variability in the ULX. Although it was not strictly necessary to simultaneously fit the spectra, we chose to do this to later allow us to assess the significance of an additional invariable MEKAL component. This model has a goodness-of-fit statistic of χ^2/degrees of freedom (dof) = 716.7/623, which cannot formally be rejected at 3σ significance. Next, we repeat the fitting process with an additional MEKAL component, which is kept constant between observations (TBABS × (TBABS × POWERLAW + MEKAL) in XSPEC). Keeping the MEKAL component fixed is reasonable if it originates in diffuse emission, although that is not necessarily the case here where we are looking at the point source. However, the data are such that we have insufficient spectral counts to constrain a variable MEKAL component, so we must make the assumption that it does not vary strongly. This additional component results in a large improvement in the goodness-of-fit over an absorbed power-law alone ($\Delta\chi^2 = 94.3$ for 2 dof). However, the 0.3–2 keV observed luminosity in the MEKAL component ($(4.1 \pm 0.4) \times 10^{38}$ erg s^{-1}) is around double that seen in the *XMM-Newton* EPIC data. Clearly, this is not physically realistic, as the putative MEKAL contribution to the *XMM-Newton* spectrum is here integrated over a much smaller area. Instead, we suggest that as the *XMM-Newton* spectrum of NGC 5408 X-1 has a two component form (e.g., Gladstone et al. 2009; Middleton et al. 2015), perhaps we are fitting the plasma emission to the soft emission component from the ULX itself, not the more subtle spectral features. Instead, a two component model of emission from a ULX may be more appropriate.

XMM-Newton ULX spectra have previously been fitted with models of emission from a multi-color-disk plus Comptonization in an optically thick medium (DISKBB + COMPTT). However, the energy response of *Chandra* ACIS is such that we could not constrain the high energy curvature, even if it was present. So, we instead opted to use a multi-color-disk with an empirical power-law approximation of Comptonization (TBABS × TBABS × SIMPL × DISKBB in XSPEC). One key difference between SIMPL and a power-law is that it does not diverge at low energies. This was potentially advantageous here, as we were trying to test for the presence of a soft, faint diffuse emission component. As previously, we simultaneously fitted the model to all eight *Chandra* spectra, with parameters free to vary between observations. Again, we did this, to allow for a comparison with an additional invariable MEKAL component. This results in a goodness-of-fit statistic of χ^2/dof = 628.2/607, which cannot be rejected at 2σ significance. From the model, we estimated inner disk temperatures of 0.17–0.22 keV and power-law spectral indices of typically 2.2–2.4, with the exception of observation 13018, which required a softer spectral index of $2.88^{+0.10}_{-0.08}$.

The addition of the MEKAL component to the two component ULX model (i.e., TBABS × (TBABS × SIMPL × DISKBB + MEKAL), Figure 5) resulted in a reduction to the fit statistic (χ^2/dof = 615.5/605; i.e., $\Delta\chi^2 = 12.7$ for 2 dof), with a plasma temperature of $0.27^{+0.03}_{-0.02}$ keV. We note that this additional spectral component is not strongly required by the *Chandra* data, however we are not testing for its significance here, we are simply constraining how much flux it could contain. Our estimate of the MEKAL temperature is in disagreement with the value of 0.87 ± 0.02 keV reported by Miller et al. (2013). However, we repeated the spectral fitting with the MEKAL temperature fixed at 0.87 keV, and compared the fits using an *F*-test. Setting the MEKAL plasma temperature in this way resulted in an increase in χ^2 of 2.2 for 1 dof. This corresponds to an *F*-test probability of 0.14, thus the improvement in the fit from allowing the plasma temperature to vary is only very marginal ($<2\sigma$ significance). We estimated the observed 0.3–2 keV luminosity of the MEKAL component using the CFLUX convolution model in XSPEC to be $L_X = 1.3^{+0.7}_{-0.4} \times 10^{38}$ erg s^{-1} (or $1.3^{+0.4}_{-0.3} \times 10^{38}$ erg s^{-1} when the MEKAL temperature was fixed to 0.87 keV). This luminosity is consistent with the point source providing the observed *XMM-Newton* putative MEKAL component that remains after subtracting the spatially resolved diffuse emission. In this model, the physical interpretation of the second TBABS component is not clear, as it accounts for both absorption in the host galaxy and intrinsic to the ULX. Therefore, at least the galactic component of this absorption should be applied to the putative plasma emission features, and arguably the intrinsic component too, depending on their physical origin. As such, we also tried TBABS × TBABS × (SIMPL × DISKBB + MEKAL), with the first absorption component set to the Galactic value and the second free to vary, but fixed between observations. In this iteration the mekal temperature was $kT = 0.25 \pm 0.02$ keV and the 0.3–2 keV observed component luminosity was slightly higher at $L_X = 2.2^{+0.4}_{-0.6} \times 10^{38}$ erg cm^{-2} s^{-1}, but is still consistent with the previous estimate. This plasma temperature is still in disagreement with the value reported by Miller et al. (2013), but the luminosity is consistent with that of the entire MEKAL component seen in *XMM-Newton* data.

3. DISCUSSION AND CONCLUSIONS

Previous *XMM-Newton* analyses of NGC 5408 X-1 have identified spectral residuals that can be modeled as emission

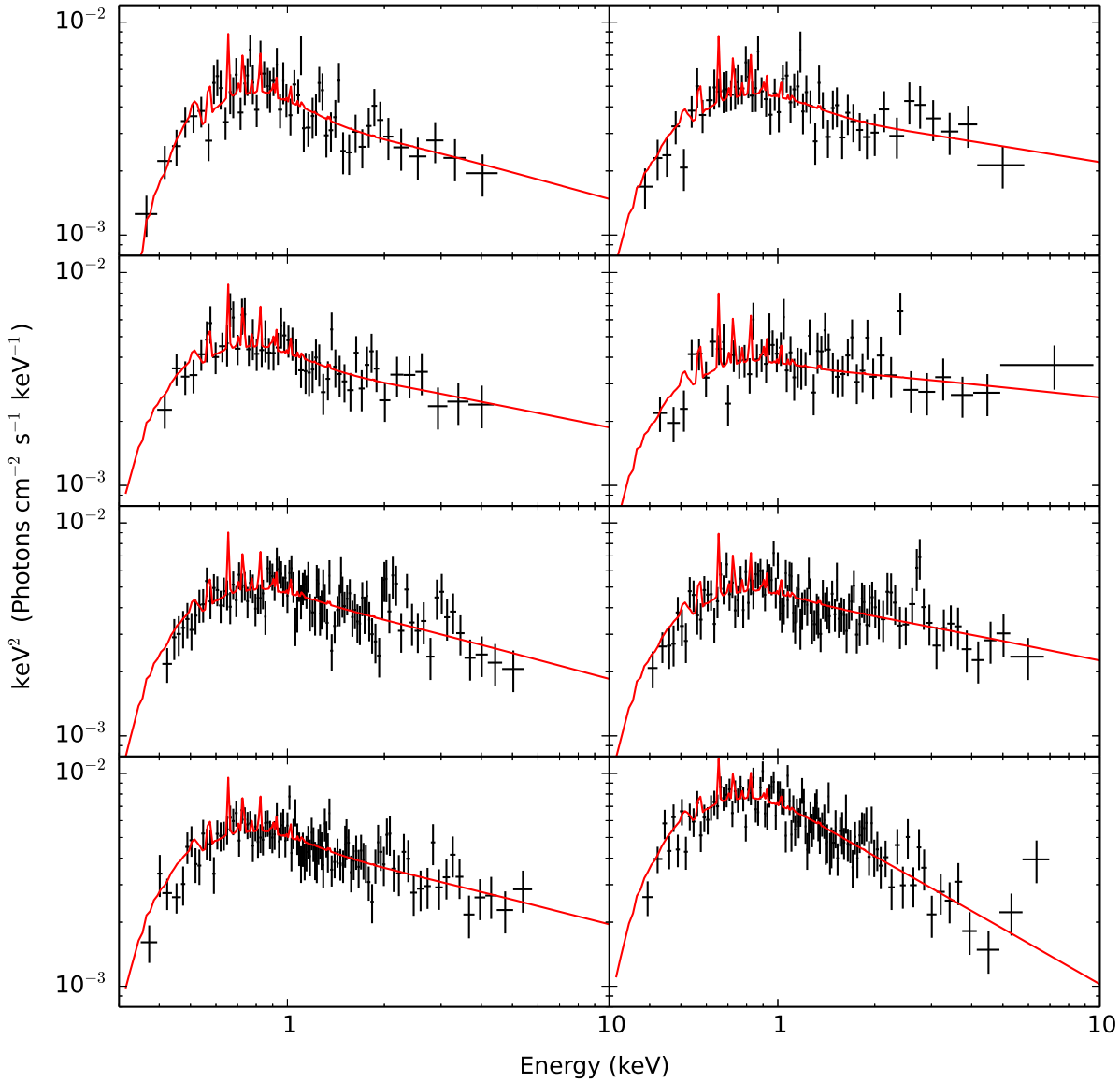

Figure 5. X-ray spectra from the eight *Chandra* ACIS-S observations detailed in Table 1. The data have been unfolded using a power-law in XSPEC with $\Gamma = 0$ and Norm $= 1$. The spectra are shown in order of observation date, starting at the top left and reading across the rows. The X-ray spectra were extracted using CIAO, and data points grouped to a minimum of 20 counts per bin, as described in the main body of text. The spectral data are over-plotted with the best fitting model of a two-component ULX continuum, with an additional contribution from diffuse plasma emission (TBAB × (TBABS × SIMPL × DISKBB + MEKAL) in XSPEC), with the plasma emission component fixed between the different observations.

from a thermal plasma. As such, it has previously been assumed that these residuals originated in star formation related diffuse emission in the host galaxy, and they were not associated with the ULX itself (e.g., Strohmayer & Mushotzky 2009; Miller et al. 2013). However, Middleton et al. (2014) noted that this would require the diffuse emission within the *XMM-Newton* source extraction region to be in excess of that expected for the entire galaxy based on its star formation rate. Instead, Middleton et al. (2014) suggested that the residuals may originate in a radiation-pressure-dominated wind coming from the ULX. In this work, we have exploited the spatial resolution of *Chandra* to place the best possible limits on the origin of the putative diffuse plasma emission.

From our analysis, we find no strong evidence that the ULX deviates from remaining essentially point-like in *Chandra* ACIS data. While a hand-full of faint point sources not evident in the *XMM-Newton* observations are resolved, the ULX does not appear to sit within a strongly peaked distribution of diffuse emission. This is not particularly unexpected, given that the ULX is largely displaced from the major star formation regions in NGC 5408. This result is also largely confirmed by a spectral analysis of the regions surrounding X-1. Although we do find an excess of counts within 30 arcsec of the ULX, these are only sufficient to account for a 0.3–2 keV luminosity of $\lesssim 7.4 \times 10^{37}$ erg s^{-1}. Admittedly, this limit is a factor $\sim$2 greater than the predicted star formation related luminosity integrated over the entirety of NGC 5408 (Middleton et al. 2014), but it may contain some degree of unresolved point source emission, and is still only sufficient to contribute $\sim 1/3$ of the 0.3–2 keV MEKAL flux seen in the *XMM-Newton* data ($\sim 2.5 \times 10^{38}$ erg s^{-1}; calculated from Miller et al. 2013).

To test whether the *Chandra* ULX point source spectra could be harbouring the remainder of the putative plasma flux observed in the *XMM-Newton* data, we fitted them with a model for the continuum spectrum from a ULX, plus an additional MEKAL component. The MEKAL component had a 0.3–2 keV luminosity of $1.3^{+0.7}_{-0.4} \times 10^{38}$ erg s^{-1} (or $1.3^{+0.4}_{-0.3} \times 10^{38}$ erg s^{-1} assuming a plasma temperature of 0.87 keV), thus is consistent with contributing the missing flux. We know from the *HST* data that a small optical association falls within the 5 arcsec source extraction region (Grisé et al. 2012), but *Chandra* sees a point source and it seems very unlikely that a minor stellar association could produce ∼4 times the diffuse X-ray emission than is expected over the entire galaxy. Indeed, we very crudely estimate the X-ray luminosity of this association as $\sim 2 \times 10^{33}$–2×10^{35} erg s^{-1} by assuming that all ∼20 of the stars are colliding wind binaries (Mauerhan et al. 2010). We note that the additional MEKAL component is not strongly required by the data, although this is hardly surprising given that it contributes only ∼4.6% of the flux (Strohmayer et al. 2007), and we are much more photon-limited here than in the *XMM-Newton* observations. Not only does *XMM-Newton* EPIC have greater effective area, but in the case of NGC 5408 X-1 the observations also have much greater exposure times: six *XMM-Newton* observations have between 28.6 and 88.2 ks of good time (Middleton et al. 2014), compared to at best 12.2 ks with *Chandra*. However, it is reasonable to include the MEKAL component here, as we have prior knowledge that two component phenomenological ULX models excluding it are ruled out by the *XMM-Newton* data (e.g., Strohmayer et al. 2007).

The majority of the putative plasma flux remains spatially unresolved, and is not displaced from the *Chandra* point source. Therefore, the putative MEKAL features in *XMM-Newton* data cannot be dominated by star formation related diffuse emission. Rather, we favor scenarios where they are associated with the ULX. Similar spectral features have been reported in a number of other ULXs, including: Ho II X-1 (Miyaji et al. 2001; Dewangan et al. 2004), NGC 4395 X-1 (Stobbart et al. 2006), NGC 4559 X-1 (Roberts et al. 2004), NGC 6946 X-1 (Middleton et al. 2014) and NGC 7424 ULX2 (Soria et al. 2006). Notably these sources all have soft X-ray spectra, at least in the observations where residuals are reported (Stobbart et al. 2006; Sutton et al. 2013; Middleton et al. 2014). Furthermore, Soria et al. (2006) reported detections of NGC 7424 ULX2 with both hard and soft spectra ($\Gamma = 1.8^{+0.2}_{-0.1}$ and 2.2 ± 0.2 respectively when fitted with absorbed power-laws), with the plasma-like component only being detected when the source had a soft spectrum, thus ruling out the possibility that it originates from underlying emission. The fact that we typically see these plasma emission-like features in ULXs with soft X-ray spectra strongly suggests that they could be associated with a super-critical wind. However, similar features have been identified in ULXs with hard X-ray spectra, e.g., NGC 1313 X-1 (Bachetti et al. 2013) and Ho IX X-1 (Walton et al. 2014). This does not necessarily rule out an association with an outflow. The wind would be expected to become physically diffuse as it moves away from the accretion disk, thus the optically thin phase could intercept an observers line of sight at low inclinations, even if the optically thick material does not. Additionally, the wind opening angle is expected to vary with accretion rate (King 2008), so ULXs could shift between hard and soft ultraluminous states. Indeed, such shifts have been reported in NGC 1313 X-1 and NGC 5204 X-1 (Sutton et al. 2013). Furthermore, Middleton et al. (2015) show that the strength of the the putative absorption features in NGC 1313 X-1 are anti-correlated with spectral hardness, which supports the interpretation that they are associated with an outflow.

One possibility, as suggested by Middleton et al. (2014), is that putative mekal features do not originate from plasma emission, rather they are misdiagnosed absorption features from a blueshifted, partially ionized, optically thin absorber. Such a material could originate from a radiation-pressure dominated wind driven by super-critical accretion, at large distances from the black hole. Alternatively, the features may truly be associated with thermal plasma emission. This could potentially occur if ejecta in the ULX wind collisionally ionize a nearby cloud of material, such as the outer-layers of a highly evolved massive stellar companion (Roberts et al. 2004). However, observational data (Middleton et al. 2011; Sutton et al. 2013; Middleton et al. 2015) and simulations (Takeuchi et al. 2013) suggest that the distinction between hard and soft ultraluminous sources is determined at least in part by the observation angle. As there is no a priori reason that such plasma emission would be anisotropic, the stronger detections in soft ultralumious ULXs is troubling for the collisionally ionized plasma emission scenario. For this reason, we tend toward favoring absorption as the more likely explanation. Future missions with high spectral resolution, such as *Astro-H* and *Athena*, will be able to provide definitive tests of the nature of the features we discuss here. However, in the meantime further diagnostics can come from examining their evolution with changing X-ray continuum spectra (Middleton et al. 2015).

We thank Douglas Swartz for useful suggestions and discussion. A.D.S. and T.P.R. acknowledge funding from the Science and Technology Facilities Council as part of the consolidated grants ST/K000861/1 and ST/L00075X/1. A.D.S. also acknowledges funding through a NASA Post-doctoral Program appointment at Marshall Space Flight Center, administered by Oak Ridge Associated Universities on behalf of NASA. M.J.M. appreciates support from ERC grant 340442.

Facility: CXO.

REFERENCES

Bachetti, M., Rana, V., Walton, D. J., et al. 2013, ApJ, 778, 163
Bachetti, M., Harrison, F. A., Walton, D. J., et al. 2014, Natur, 514, 202
Colbert, E. J. M., & Mushotzky, R. F. 1999, ApJ, 519, 89
Dale, D. A., Bendo, G. J., Engelbracht, C. W., et al. 2005, ApJ, 633, 857
Davis, J. E., Bautz, M. W., Dewey, D., et al. 2012, Proc. SPIE, 8443, 84431A
Dewangan, G. C., Miyaji, T., Griffiths, R. E., & Lehmann, I. 2004, ApJL, 608, L57
Dickey, J. M., & Lockman, F. J. 1990, ARA&A, 28, 215
Evans, I. N., Primini, F. A., Glotfelty, K. J., et al. 2010, ApJS, 189, 37
Gladstone, J. C., Roberts, T. P., & Done, C. 2009, MNRAS, 397, 1836
Grimm, H.-J., Gilfanov, M., & Sunyaev, R. 2003, MNRAS, 339, 793
Grisé, F., Kaaret, P., Corbel, S., Cseh, D., & Feng, H. 2013, MNRAS, 433, 1023
Grisé, F., Kaaret, P., Corbel, S., et al. 2012, ApJ, 745, 123
Kaaret, P., Corbel, S., Prestwich, A. H., & Zezas, A. 2003, Sci, 299, 365
Kaaret, P., & Feng, H. 2009, ApJ, 702, 1679
Kajava, J. J. E., & Poutanen, J. 2009, MNRAS, 398, 1450
Kajava, J. J. E., Poutanen, J., Farrell, S. A., Grisé, F., & Kaaret, P. 2012, MNRAS, 422, 990
Karachentsev, I. D., Sharina, M. E., Dolphin, A. E., et al. 2002, A&A, 385, 21
Kawashima, T., Ohsuga, K., Mineshige, S., et al. 2012, ApJ, 752, 18
King, A. R. 2004, MNRAS, 347, L18

King, A. R. 2008, MNRAS, 385, L113
King, A. R. 2009, MNRAS, 393, L41
Liu, J.-F., Bregman, J. N., Bai, Y., Justham, S., & Crowther, P. 2013, Natur, 503, 500
Lucy, L. B. 1974, AJ, 79, 745
Mapelli, M., Ripamonti, E., Zampieri, L., Colpi, M., & Bressan, A. 2010, MNRAS, 408, 234
Mauerhan, J. C., Muno, M. P., Morris, M. R., Stolovy, S. R., & Cotera, A. 2010, ApJ, 710, 706
Middleton, M. J., Heil, L., Pintore, F., Walton, D. J., & Roberts, T. P. 2015, MNRAS, 447, 3243
Middleton, M. J., Miller-Jones, J. C. A., Markoff, S., et al. 2013, Natur, 493, 187
Middleton, M. J., Roberts, T. P., Done, C., & Jackson, F. E. 2011, MNRAS, 411, 644
Middleton, M. J., Walton, D. J., Fabian, A., et al. 2015, MNRAS, 454, 3134
Middleton, M. J., Walton, D. J., Roberts, T. P., & Heil, L. 2014, MNRAS, 438, L51
Miller, J. M., Walton, D. J., King, A. L., et al. 2013, ApJL, 776, L36
Mineo, S., Gilfanov, M., & Sunyaev, R. 2012, MNRAS, 419, 2095
Miyaji, T., Lehmann, I., & Hasinger, G. 2001, AJ, 121, 3041
Motch, C., Pakull, M. W., Soria, R., Grisé, F., & Pietrzyński, G. 2014, Natur, 514, 198
Pasham, D. R., & Strohmayer, T. E. 2012, ApJ, 753, 139
Poutanen, J., Lipunova, G., Fabrika, S., Butkevich, A. G., & Abolmasov, P. 2007, MNRAS, 377, 1187
Richardson, W. H. 1972, JOSA, 62, 55
Roberts, T. P., Warwick, R. S., Ward, M. J., & Goad, M. R. 2004, MNRAS, 349, 1193
Shakura, N. I., & Sunyaev, R. A. 1973, A&A, 24, 337
Soria, R., Kuncic, Z., Broderick, J. W., & Ryder, S. D. 2006, MNRAS, 370, 1666
Soria, R., Motch, C., Read, A. M., & Stevens, I. R. 2004, A&A, 423, 955
Stobbart, A.-M., Roberts, T. P., & Wilms, J. 2006, MNRAS, 368, 397
Strohmayer, T. E. 2009, ApJL, 706, L210
Strohmayer, T. E., & Mushotzky, R. F. 2009, ApJ, 703, 1386
Strohmayer, T. E., Mushotzky, R. F., Winter, L., et al. 2007, ApJ, 660, 580
Sutton, A. D., Roberts, T. P., & Middleton, M. J. 2013, MNRAS, 435, 1758
Takeuchi, S., Ohsuga, K., & Mineshige, S. 2013, PASJ, 65, 88
Walton, D. J., Harrison, F. A., Grefenstette, B. W., et al. 2014, ApJ, 793, 21
Walton, D. J., Miller, J. M., Harrison, F. A., et al. 2013, ApJL, 773, L9
Walton, D. J., Miller, J. M., Reis, R. C., & Fabian, A. C. 2012, MNRAS, 426, 473
Wilms, J., Allen, A., & McCray, R. 2000, ApJ, 542, 914
Zampieri, L., & Roberts, T. P. 2009, MNRAS, 400, 677